CrossMark

J. Fluid Mech. (2016), *vol.* 802, *pp.* 245–262. © Cambridge University Press 2016
doi:10.1017/jfm.2016.447

Dynamics of ferrofluid drop deformations under spatially uniform magnetic fields

P. Rowghanian[1], C. D. Meinhart[1] and O. Campàs[1,†]

[1]Department of Mechanical Engineering, and California NanoSystems Institute, University of California, Santa Barbara, CA 93106, USA

(Received 4 March 2016; revised 1 June 2016; accepted 27 June 2016; first published online 3 August 2016)

We systematically study the shape and dynamics of a Newtonian ferrofluid drop immersed in an immiscible, Newtonian and non-magnetic viscous fluid under the action of a uniform external magnetic field. We obtain the exact equilibrium drop shapes for arbitrary ferrofluids, characterize the extent of deviations of the exact shape from the commonly assumed ellipsoidal shape, and analyse the smoothness of highly curved tips in elongated drops. We also present a comprehensive study of drop deformation for a Langevin ferrofluid. Using a computational scheme that allows fast and accurate simulations of ferrofluid drop dynamics, we show that the dynamics of drop deformation by an applied magnetic field is described up to a numerical factor by the same time scale as drop relaxation in the absence of any magnetic field. The numerical factor depends on the ratio of viscosities and the ratio of magnetic to capillary stresses, but is independent of the nature of the ferrofluid in most practical cases.

Key words: drops, magnetic fluids

1. Introduction

Droplet shape deformations have been extensively studied in many different contexts, both at the fundamental level and also for specific applications with industrial and biomedical relevance that require a good understanding of how droplets deform. Starting from the pioneering work of Taylor (1934), deformation of fluid drops by shear flows of Newtonian (Cox 1969; Schmitz & Felderhof 1982; Rallison 1984; Tretheway & Leal 2001) and complex (Chilcott & Rallison 1988; Ramaswamy & Leal 1999; Zhou *et al.* 2010) fluids has been extensively studied. These studies have important implications for several problems, such as emulsion flows as well as many industrial applications, including food processing, pharmaceutical manufacturing, etc. (Nielloud & Marti-Mestres 2000; Friberg, Larsson & Sjoblom 2003; Sjoblom 2005). In addition to the studies of droplet deformation and dynamics in shear flows, various works have focused on drop deformations generated by body forces, including drops deformed under the action of electric (Allan & Mason 1962; Taylor 1964; Rosenkilde 1969; Miksis 1981; Wohlhuter & Basaran 1992) and magnetic (Bacri & Salin 1982; Sero-Guillaume *et al.* 1992) fields.

† Email address for correspondence: campas@engineering.ucsb.edu

https://doi.org/10.1017/jfm.2016.447 Published online by Cambridge University Press

The theoretical study of drop deformation under an applied electric field for nearly spherical drops (Allan & Mason 1962) provided important insights into the subject. Equilibrium deformation and stability of conducting (Taylor 1964) and linear dielectric (Rosenkilde 1969) drops under an electric field were then studied assuming ellipsoidal drop shapes for small to moderate deformations. Relaxing the ellipsoidal shapes assumption, the axisymmetric shapes and stability of linear (Miksis 1981; Wohlhuter & Basaran 1992) and nonlinear (Basaran & Wohlhuter 1992; Wohlhuter & Basaran 1993) dielectric drops were studied numerically. All these works reported bistable drop shapes (Bacri & Salin 1982) above a certain threshold of relative permittivity of drops to the surrounding media.

Described by equations mathematically equivalent to those governing uncharged dielectric drops, the deformations of ferrofluid drops (Rosensweig 2013) under the effect of magnetic fields have also been independently studied. Deformation of linear ferrofluid drops was studied for small (Arkhipenko, Barkov & Bashtovoi 1979; Tsebers 1985) and finite (Afkhami *et al.* 2010) deformations by assuming ellipsoidal shapes. The exact equilibrium shapes of linear ferrofluid drops under the action of a magnetic field were then obtained numerically, and large mean curvature at the tips compared to that of ellipsoids was reported (Sero-Guillaume *et al.* 1992). The exact equilibrium shapes of linear ferrofluid on a solid surface were also studied experimentally (Zhu *et al.* 2011). The bistability of equilibrium drop shapes above a certain ferrofluid susceptibility, which was first observed by Bacri & Salin (1982) for ferrofluid drops, was later observed also for dielectric drops. This observed bistability in ferrofluid drop equilibrium shapes was studied numerically for linear ferrofluid drops (Lavrova *et al.* 2004, 2006).

The dynamics and stability of dielectric and magnetic fluids have been studied under diverse conditions. Destabilization of the interface between a ferrofluid and a non-magnetic fluid was discussed first by Boudouvis *et al.* (1987), and explored further by Engel, Langer & Chetverikov (1999), Abou, Wesfreid & Roux (2000), Lavrova *et al.* (2006), Gollwitzer *et al.* (2007), Chen & Cheng (2008), Mizuta (2011) and Cao & Ding (2014). Multiple works studied the breakup of drops under electric (Sherwood 1988; Basaran *et al.* 1995; Lac & Homsy 2007; Deshmukh & Thaokar 2012; Paknemat, Pishevar & Pournaderi 2012; Karyappa, Naik & Thaokar 2015) or magnetic (Potts, Barrett & Diver 2001; Afkhami *et al.* 2008) fields, as well as the breakup of jets under electric fields (Collins, Harris & Basaran 2007). Drop formation facilitated by electric (Notz & Basaran 1999) and magnetic (Chen, Chen & Lee 2009) fields, and dynamics and instabilities of pendent drops under an electric field (Acero *et al.* 2013; Ferrera *et al.* 2013; Corson *et al.* 2014) were also explored. Other works addressed simultaneous motion and deformation of free drops under magnetic fields (Nguyen, Ng & Huang 2006; Shi, Bi & Zhou 2014), electrified drops in a microfluidic channel (Wehking & Kumar 2015), and drops on a solid surface by electric (Datta, Das & Das 2015) and rotating magnetic (Zakinyan, Nechaeva & Dikansky 2012) fields. The response of free ferrofluid drops to rotating magnetic fields (Bacri, Cebers & Perzynski 1994; Rhodes *et al.* 2006; Cebers & Kalis 2012), and the formation of complex drop shapes due to AC and rotating magnetic fields (Rhodes *et al.* 2006) were also considered.

While most works on electrically deformed dielectric drops assume dielectric surrounding media (with a few exceptions, which consider non-polarizable surrounding media (Pillai *et al.* 2015)), the vast majority of theoretical and numerical studies of free ferrofluid drops have focused on the limit of non-magnetic surrounding media. The relative simplicity of the stress equations in this limit, and its wide applicability

https://doi.org/10.1017/jfm.2016.447 Published online by Cambridge University Press

in the case of ferrofluid drops due to the weak magnetic response of most fluids, make the limit of non-magnetic surrounding media very interesting in many practical cases. In addition, this limit affects the stability conditions of the drops. In the case of dielectric media, drops become unstable for large enough electric fields (Taylor 1964; Rosenkilde 1969; Miksis 1981; Wohlhuter & Basaran 1992) above a threshold of relative permittivity (different from the bistability threshold). The instability is due to the development of sharp conical tips at the drop poles (Sherwood 1991; Li, Halsey & Lobkovsky 1994; Stone, Lister & Brenner 1999), which form due to the divergence of the electric field at the tips and cause the ejection of jets from those ends (Taylor 1964; Collins *et al.* 2007; Ferrera *et al.* 2013). In the limit of non-magnetic (non-polarizable) media, conical shapes and resulting instabilities appear only under extreme conditions, where the field at the poles becomes so large that the magnetization (polarization) of the medium at the poles cannot be neglected any more. For ferrofluid drops in external media with negligible magnetic response, as is the case in most practical conditions, this instability does not occur.

Despite the variety of studies on drop deformations and dynamics so far, there are only a handful of works that consider drop actuation under uniform electric fields. Specifically, Basaran *et al.* (1995) and Feng & Scott (1996) studied the dynamics of drops subject to instantaneous increase or decrease, as well as oscillations, of electric fields, and Feng & Scott (1996) studied the fluid flow inside and outside drops under electric fields. Esmaeeli & Sharifi (2011*a*,*b*) found the actuation time scale for small deformations, and Mandal, Chaudhury & Chakraborty (2014) studied how the actuation time scale was affected by charge accumulation on the drop surface. In contrast to electric actuation of droplets, the dynamics of ferrofluid drops in non-magnetic external media actuated by uniform magnetic fields have not been studied before, even though it has implications for an increasing number of modern biomedical applications (Gupta & Gupta 2005; Kumar & Mohammad 2011; Laurent *et al.* 2011; Bychkova *et al.* 2012; Shapiro *et al.* 2015).

The goal of the present work is to systematically study the dynamics of a Newtonian ferrofluid drop suspended in an immiscible, non-magnetic and viscous Newtonian medium when actuated by a spatially uniform magnetic field at low Reynolds numbers. To put our results in perspective, we first obtain numerically the equilibrium drop shapes for finite drop deformations and arbitrary ferrofluids (both linear and nonlinear ferrofluids) as a function of the only relevant dimensionless parameter, namely the ratio of magnetic to capillary stresses. We show that equilibrium drop shapes differ significantly from ellipsoidal shapes when magnetic stresses are large compared to capillary stresses, and investigate the deviation from ellipsoidal shapes numerically and also analytically, by expanding the shapes in terms of spherical harmonics. We derive the region of the parameter space with drop shape bistability, and show that there exists a minimal magnetic susceptibility below which shape bistability is never observed. We then study the dynamics of drop relaxation and actuation by an external uniform magnetic field in nonlinear ferrofluid regimes and for finite drop deformations. We show that, for small drop deformations, the time scale of drop deformation upon actuation with a uniform magnetic field is the same as the relaxation time scale of an initially deformed drop driven by capillary stresses. For larger deformations, the actuation time differs from the relaxation time by a numerical factor, which depends on the ratio of drop to medium viscosities and the ratio of magnetic to capillary stresses, but is largely independent of the nature of the ferrofluid. Importantly, we develop a computational scheme using COMSOL Multiphysics V5.0 (www.comsol.com) that allows computationally efficient

https://doi.org/10.1017/jfm.2016.447 Published online by Cambridge University Press

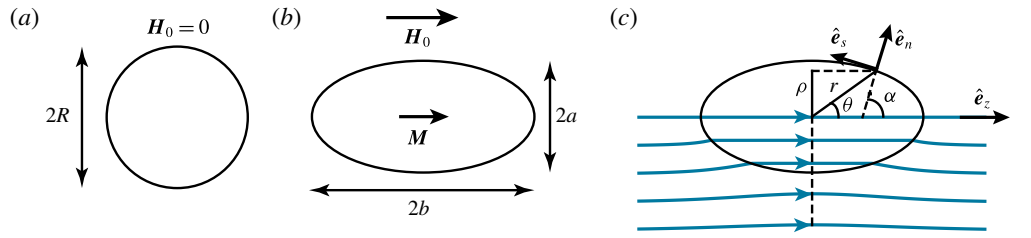


FIGURE 1. (Colour online) Sketch of a ferrofluid drop in the absence (*a*) and presence (*b*) of an external uniform magnetic field $\boldsymbol{H}_0$. The drop elongates axisymmetrically along the direction of $\boldsymbol{H}_0$. (*c*) Magnetic field lines around the deformed ferrofluid drop (lower half), and parametrization of the drop shape (top half).

simulations of drops deformed by stresses acting at the drop interface, as is the case for drops actuated by electric and magnetic fields as well as drops deformed by active surrounding media. We believe this computational scheme will benefit basic and applied research, which require fast and accurate simulations of drops deformed by stresses acting at the drop interface.

2. Theoretical description

We consider a Newtonian and incompressible ferrofluid drop of radius R and viscosity η_d immersed in a Newtonian and incompressible fluid of viscosity η_m. For simplicity, we assume any anisotropy in ferrofluid viscosity to be negligible, which is the case in most ferrofluids at low enough ferromagnetic nanoparticle concentrations (Shliomis 1972). Upon the application of a spatially uniform external magnetic field $\boldsymbol{H}_0 = H_0\hat{\boldsymbol{e}}_z$, the ferrofluid drop magnetizes and deforms axisymmetrically along the direction of the applied field (figure 1). We parametrize the axisymmetric drop shape using cylindrical coordinates and the angle α of the outward normal $\hat{\boldsymbol{e}}_n$ to the drop surface with the axis of symmetry ($\cos\alpha = \hat{\boldsymbol{e}}_n \cdot \hat{\boldsymbol{e}}_z$; figure 1*c*). Defining s as the arclength along the drop interface, the principle curvatures of the drop interface κ_s and κ_ϕ along the directions $\hat{\boldsymbol{e}}_s$ and $\hat{\boldsymbol{e}}_\phi$ read $\kappa_s = \mathrm{d}\alpha/\mathrm{d}s = \cos\alpha\,\mathrm{d}\alpha/\mathrm{d}\rho$ and $\kappa_\phi = \sin\alpha/\rho$, respectively.

In the low-Reynolds-number limit considered here, the shape and dynamics of the drop result from local stress balance, fluid incompressibility in the bulk and the evolution of the magnetic field $\boldsymbol{H}$, together with boundary conditions for the hydrodynamic and magnetic fields at the drop interface. Local stress balance and fluid incompressibility read

$$\nabla \cdot (\boldsymbol{\sigma}^h + \boldsymbol{\sigma}^m) = 0, \quad \nabla \cdot \boldsymbol{u} = 0, \tag{2.1a,b}$$

where $\boldsymbol{\sigma}^h$ and $\boldsymbol{\sigma}^m$ are the hydrodynamic and magnetic stress tensors (defined below), respectively, and $\boldsymbol{u}$ is the fluid velocity field. Assuming that the magnetic field relaxes much faster than any other dynamical processes in the system (magnetostatic approximation, valid for dilute ferrofluids), the magnetic field $\boldsymbol{H}$ and magnetic flux density $\boldsymbol{B}$ follow the magnetostatic equations, namely

$$\nabla \cdot \boldsymbol{B} = 0, \quad \nabla \times \boldsymbol{H} = 0. \tag{2.2a,b}$$

https://doi.org/10.1017/jfm.2016.447 Published online by Cambridge University Press

Stress balance and continuity of velocity, tangential magnetic field and normal magnetic flux density at the drop interface impose the following boundary conditions:

$$[[\hat{\boldsymbol{e}}_n \cdot (\boldsymbol{\sigma}^h + \boldsymbol{\sigma}^m) \cdot \hat{\boldsymbol{e}}_n]] = \gamma(\kappa_s + \kappa_\phi), \tag{2.3}$$

$$[[\hat{\boldsymbol{e}}_s \cdot (\boldsymbol{\sigma}^h + \boldsymbol{\sigma}^m) \cdot \hat{\boldsymbol{e}}_n]] = 0, \tag{2.4}$$

$$[[\boldsymbol{u}]] = 0, \quad \boldsymbol{u}_{int} = (\hat{\boldsymbol{e}}_n \cdot \boldsymbol{u})\hat{\boldsymbol{e}}_n, \tag{2.5}$$

$$[[\boldsymbol{H} \cdot \hat{\boldsymbol{e}}_s]] = 0, \quad [[\boldsymbol{B} \cdot \hat{\boldsymbol{e}}_n]] = 0, \tag{2.6}$$

where γ is the interfacial tension between the ferrofluid and its surrounding medium, $\boldsymbol{u}_{int}$ is the interface velocity, and the notation $[[x]] \equiv x_{out} - x_{in}$ indicates the discontinuity of the quantity x at the interface. The continuity of tangential magnetic field and normal magnetic flux density (2.6) is due to the magnetostatic approximation (no ϕ component considered due to the axial symmetry).

Given that both the ferrofluid drop and the continuous medium surrounding it are Newtonian fluids, the hydrodynamic stress tensor reads

$$\boldsymbol{\sigma}^h = -P\boldsymbol{I} + \eta\dot{\boldsymbol{\epsilon}}, \tag{2.7}$$

where $\boldsymbol{I}$ is the unit tensor, P the hydrostatic pressure, η the fluid viscosity ($\eta = \eta_d$ for the drop and $\eta = \eta_m$ for the external medium) and $\dot{\boldsymbol{\epsilon}} = (\boldsymbol{\nabla u} + \boldsymbol{\nabla u}^{\mathrm{T}})/2$ the strain-rate tensor. In the magnetostatic approximation, the magnetic stress inside the ferrofluid drop is given by (Stierstadt & Liu 2015)

$$\boldsymbol{\sigma}^m = -\mu_0 \left(\frac{1}{2}\boldsymbol{H}^2 + \int_0^H \boldsymbol{M}(\boldsymbol{H}) \cdot \mathrm{d}\boldsymbol{H} \right) \boldsymbol{I} + \boldsymbol{H} \otimes \boldsymbol{B}, \tag{2.8}$$

where μ_0 is the vacuum magnetic permeability and $\boldsymbol{M}$ is the drop magnetization.

Both in the external non-magnetic medium and inside the ferrofluid drop, $\boldsymbol{\nabla} \cdot \boldsymbol{\sigma}^m = 0$. In the non-magnetic external medium, $\boldsymbol{\nabla} \cdot \boldsymbol{\sigma}^m = -\boldsymbol{\nabla} B^2/(2\mu_0) + (\boldsymbol{B} \cdot \boldsymbol{\nabla})\boldsymbol{B}/\mu_0$, which vanishes because $\boldsymbol{\nabla} \times \boldsymbol{B} = 0$. Inside the drop, the term vanishes because the ferrofluid contains dispersed mobile ferromagnetic particles that impose uniform magnetic field and magnetization inside the drop. Furthermore, the magnetic shear stress at the interface, which reads $[[\hat{\boldsymbol{e}}_s \cdot \boldsymbol{\sigma}^m \cdot \hat{\boldsymbol{e}}_n]] = [[(\boldsymbol{H} \cdot \hat{\boldsymbol{e}}_s)(\boldsymbol{B} \cdot \hat{\boldsymbol{e}}_n)]]$, vanishes because the tangential component of $\boldsymbol{H}$ and the normal component of $\boldsymbol{B}$ are continuous at the drop interface (2.6). In contrast to ferrofluid drops, in which the normal component of the magnetic flux density is always continuous at the drop interface due to the non-existence of magnetic charges, the analogous continuity is not satisfied for weakly conducting (leaky) dielectric drops under electric fields because of electric charge accumulation at the interface (see Melcher & Taylor (1969) and Saville (1997) for reviews). Under those conditions, the electric shear stress on the interface does not vanish, which results in fluid flows and affects the drop shapes (Lac & Homsy 2007; Salipante & Vlahovska 2010; Lanauze, Walker & Khair 2015).

Using the expressions (2.7) and (2.8) for the hydrodynamic and magnetic stress tensors as well as the simplifications described above, equations (2.3) and (2.4) reduce to

$$[[\hat{\boldsymbol{e}}_n \cdot \boldsymbol{\sigma}^m \cdot \hat{\boldsymbol{e}}_n]] - [[P]] + [[\eta\hat{\boldsymbol{e}}_n \cdot \dot{\boldsymbol{\epsilon}} \cdot \hat{\boldsymbol{e}}_n]] = \gamma(\kappa_s + \kappa_\phi), \tag{2.9}$$

$$[[\eta\hat{\boldsymbol{e}}_s \cdot \dot{\boldsymbol{\epsilon}} \cdot \hat{\boldsymbol{e}}_n]] = 0. \tag{2.10}$$

2.1. *Scales and dimensionless parameters*

We scale all length scales with the radius R of the initial undeformed drop, all stresses with the capillary stress scale $\sigma_c = \gamma/R$, and time with the relaxation time scale $\tau_m \equiv \eta_m/\sigma_c$. Equation (2.9), which embodies the local normal stress balance at the

https://doi.org/10.1017/jfm.2016.447 Published online by Cambridge University Press

drop interface, can then be expanded and rewritten in the following dimensionless form:

$$\beta \cos^2\alpha + Q(\tilde{\rho}) + \hat{\boldsymbol{e}}_n \cdot \dot{\tilde{\boldsymbol{\epsilon}}}_m \cdot \hat{\boldsymbol{e}}_n - \lambda\, \hat{\boldsymbol{e}}_n \cdot \dot{\tilde{\boldsymbol{\epsilon}}}_d \cdot \hat{\boldsymbol{e}}_n = \frac{\mathrm{d}\alpha}{\mathrm{d}\tilde{\rho}} \cos\alpha + \frac{\sin\alpha}{\tilde{\rho}}, \tag{2.11}$$

where the ratio $\beta \equiv \sigma_m/\sigma_c$ of the magnetic stress scale $\sigma_m \equiv \mu_0 M^2(H)/2$ to the capillary stress scale, and the ratio $\lambda \equiv \eta_d/\eta_m$ of the fluid viscosities inside and outside the drop, are the only dimensionless parameters in the problem and fully determine its solutions. The variable $Q \equiv (\sigma_i - [[P]])/\sigma_c$, which corresponds to the normalized sum of the hydrostatic pressure discontinuity at the interface and an isotropic magnetic stress term $\sigma_i \equiv \mu_0 \int_0^H M\,\mathrm{d}H$, is determined by imposing drop volume conservation and is thus a function of β and λ. Because the surrounding medium is non-magnetic, the magnetic stress, σ_m, depends only on the uniform magnetization and magnetic field inside the drop.

3. Exact equilibrium drop shapes

In equilibrium, the fluid flows inside and outside the drop vanish and the pressure equilibrates inside and outside the drop. In these conditions, equation (2.11) reduces to

$$\beta \cos^2\alpha + Q = \frac{\mathrm{d}\alpha}{\mathrm{d}\tilde{\rho}} \cos\alpha + \frac{\sin\alpha}{\tilde{\rho}}. \tag{3.1}$$

Solutions of (3.1) depend solely on β, as the viscosity ratio λ does not play any role in the absence of fluid flows. The variable Q, now uniform along the interface, is a parameter determined by imposing drop volume conservation and depends only on β.

We obtain the exact equilibrium shapes of the drop for different values of β by numerically integrating (3.1). Starting from nearly spherical shapes for $\beta \ll 1$, drops become increasingly deformed as β increases and take approximately ellipsoidal shapes for small to moderate deformations. For large values of β, corresponding to large drop deformations (figure 2*a*), drops increasingly deviate from ellipsoidal shapes, especially at their poles, as reported by Sero-Guillaume *et al.* (1992). We analyse this deviation by calculating the difference $\Delta H_m = H_m - H_m^{ell}$ between the local mean curvature H_m of the exact equilibrium drop shape and the mean curvature H_m^{ell} of an ellipsoid with the same semiaxes (figure 2*c*). The spatial dependence of the mean curvature and its value at the pole H_m^{pole} as a function of β are also given in figures 2(*d*) and 2(*e*), respectively.

The equilibrium aspect ratio $\Delta_{eq} \equiv b/a$ of the drops, with b and a being the major and minor semiaxes, respectively, is shown in figure 2(*b*). These results are in agreement with recent works on electrically deformed drops (Pillai *et al.* 2015) and show that assuming ellipsoidal drop shapes (dashed line in figures 2*b*) results in a significant overestimation of aspect ratio for moderate to large values of β, namely $\beta \gtrsim 10$ (or aspect ratios $\Delta_{eq} \gtrsim 4$).

Important insight on how close the exact equilibrium drop shapes are to ellipsoids for small and moderate values of $\beta \gtrsim 1$, analysed above numerically by considering the differences in local curvatures, can be gained by analytical analysis. Specifically, we expand the shape function $\tilde{r}$ in terms of the spherical harmonics $Y_\ell^m(\theta, \phi)$, where $\tilde{r} \equiv r/R$, θ and ϕ are the dimensionless radial distance, polar angle and azimuthal angle, with respect to the centre of the drop. Such expansions have been employed in

https://doi.org/10.1017/jfm.2016.447 Published online by Cambridge University Press

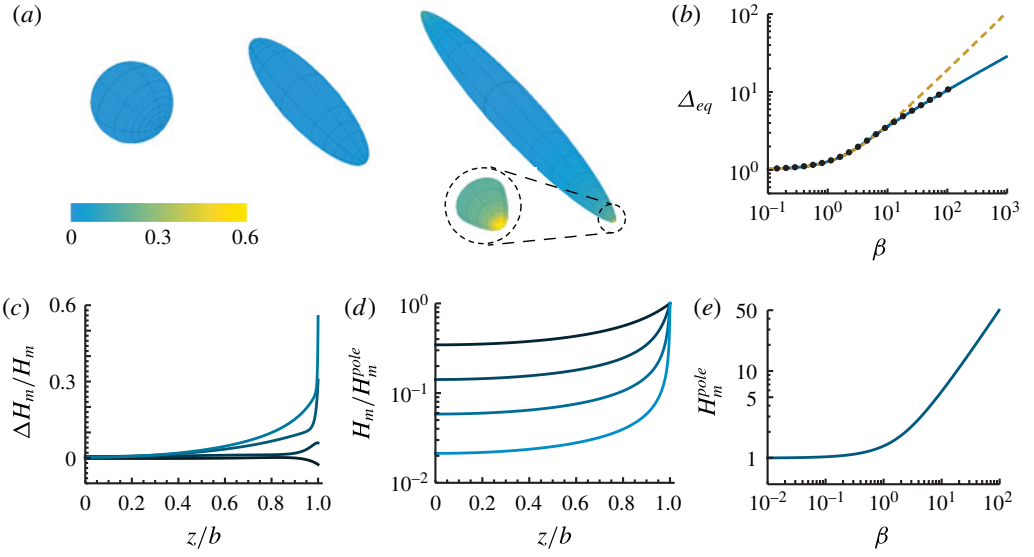


FIGURE 2. (Colour online) (*a*) Equilibrium drop shapes for $\beta = 0$, 10, 100 (left, middle, right). (*b*) Aspect ratio of equilibrium drop shapes, Δ_{eq}, as a function of β for the numerically obtained exact drop shapes (solid blue line), assuming an ellipsoidal drop shapes (dashed yellow line), and for the drop shape obtained from simulations (black dots, see next section). (*c*) Relative deviation $\Delta H_m/H_m$ of local mean curvature H_m from that of an ellipsoid for $\beta = 3$, 10, 30, 100 (dark to light), which also corresponds to the colour coding of the drop surface in (*a*). (*d*) Spatial dependence of the local mean curvature H_m normalized by the mean curvature H_m^{pole} at the pole ($z/b = 1$) for $\beta = 3$, 10, 30, 100 (dark to light). (*e*) Mean curvature at the pole, H_m^{pole}, as a function of β. For large β, $H_m^{pole} \approx \beta/2$.

previous works to study the dynamics of drops under sudden increase or decrease, as well as oscillations, of electric fields (Basaran *et al.* 1995), the motion of bubbles in inviscid fluids (Meiron 1989; Kushch *et al.* 2002) and the stability of bubbles under electric fields (Shaw & Spelt 2009). Owing to the axial and mirror symmetry of the drop, the expansion must be ϕ-independent, and consist only of $m = 0$ and even $\ell = 2j$ modes, where j is a non-negative integer. Therefore, $\tilde{r}(\theta) = 1 + \sum_{j=0}^{\infty} y_{2j}(\beta) Y_{2j}^0(\theta)$, where the coefficients y_{2j} are zero when $\beta = 0$. Truncating the series at $j = 3$ and expanding the coefficients $y_{2j}(\beta)$ up to third order in β, the normal stress balance (equation (3.1) rewritten in spherical coordinates) and drop volume conservation yield

$$\tilde{r}(\theta) \simeq 1 + \frac{\sqrt{\pi}}{90}\left(-\beta^2 + \frac{2}{63}\beta^3\right) Y_0^0(\theta) + \frac{1}{3}\sqrt{\frac{\pi}{5}}\left(\beta - \frac{1}{42}\beta^2 - \frac{8}{315}\beta^3\right) Y_2^0(\theta) + \frac{13\sqrt{\pi}}{945}\left(\beta^2 - \frac{9}{286}\beta^3\right) Y_4^0(\theta) + \left(\sqrt{\frac{\pi}{13}}\frac{197}{41\,580}\beta^3\right) Y_6^0(\theta). \tag{3.2}$$

All spherical harmonics up to order $\ell = 6$ have amplitudes of order β^2 or higher with small numerical coefficients, except for the ellipsoidal mode $\ell = 2$, which has an amplitude of order β. Comparison of the β-dependent coefficients (up to $\ell = 6$) indicates that it is safe to assume ellipsoidal drop shapes for $\beta \lesssim 5$. Major deviations of the ellipsoidal shape start occurring at $\beta \simeq 10$ (corresponding to aspect ratios ~ 4), which agrees with our numerical calculations and simulations (figure 2*c*).

https://doi.org/10.1017/jfm.2016.447 Published online by Cambridge University Press

3.1. *Equilibrium drop shape as a function of the externally applied magnetic field*

So far we have discussed the equilibrium drop shapes as a function of β, the ratio of magnetic stress to the capillary stress scale. This analysis is generic, as it does not involve the specific magnetic properties of the ferrofluid. However, some interesting aspects of drop deformations are revealed when drop deformations are analysed as a function of the experimentally controlled external magnetic field H_0 and the specific magnetic properties of the ferrofluid. It is known, for instance, that above a certain threshold of relative magnetic permeability (permittivity) of the drop to the medium, drop shapes become bistable for a range of magnetic (electric) fields (Taylor 1964; Rosenkilde 1969; Miksis 1981; Bacri & Salin 1982; Wohlhuter & Basaran 1992). These studies also show that, for dielectric drops, equilibrium solutions cease to exist altogether above a certain threshold of relative permittivity and electric field, effectively making large deformations unstable for drops with high permittivity. This instability results from the formation of conical poles (Sherwood 1991; Li *et al.* 1994; Stone *et al.* 1999) due to the divergence of the electric field just outside the drop at the poles.

To study these effects in magnetically actuated ferrofluid drops, we analyse the deformations of nonlinear ferrofluid drops as a function of the externally applied uniform magnetic field. In order to obtain the equilibrium drop shapes as a function of the applied field, it is necessary to know the dependence of the magnetization M of the specific ferrofluid used on the applied magnetic field. The ferromagnetic properties of the ferrofluid depend on the physicochemical properties of the magnetic nanoparticles dispersed in the drop phase. In the absence of hysteresis (small interaction energy between nanoparticles), the ferrofluid drop can be effectively described by its magnetization $M(H) = M_s \mathscr{L}(H/H_c)$, where H is the magnetic field inside the drop and M_s and H_c are the saturation magnetization and the saturating field, respectively. In what follows, we assume Langevin magnetization, $\mathscr{L}(x) \equiv \coth x - 1/x$ (Rosensweig 2013), which describes accurately ferrofluids with monodisperse magnetic particles. This function also captures qualitatively the behaviour of more general cases of polydisperse magnetic particles, where the magnetization relation is found by integrating over multiple Langevin functions, which correspond to the particle sizes present in the ferrofluid (Zimny *et al.* 2014). As the volume fraction of particles and the interaction energy per volume between particles increase, hysteresis effects appear and the applicability of the Langevin model becomes more limited. The effects of hysteresis in the ferrofluid magnetization on the drop shapes and dynamics are not studied here and are left to future work.

The magnetization M of the drop is a function of the magnetic field $H = H_0 + H_{in}$ inside the drop, where the induced magnetic field $H_{in} = -kM$ depends on the magnetic field H via M and the drop shape-dependent demagnetization factor k, which is maximal ($k = 1/3$) for spherical drops and decreases monotonically for increasing drop deformations. The magnetic field in the drop, $H = H_0 - kM_s \mathscr{L}(H/H_c)$, is thus given implicitly as a function of the external magnetic field H_0 and the demagnetization factor k, which we have calculated numerically for the exact equilibrium drop shapes using standard methods (Landau, Pitaevskii & Lifshitz 1984). This implicit relation introduces a dimensionless parameter $\mu \equiv M_s/H_c$, which depends only on the properties of the ferrofluid. While equilibrium drop shapes depend uniquely on β, relating these shapes to H_0 requires two parameters, namely, μ and $\beta_s \equiv \mu_0 M_s^2 R/2\gamma$, where β_s is the maximal value of $\beta = \beta_s \mathscr{L}^2(H/H_c)$ at the saturation magnetization of the ferrofluid.

https://doi.org/10.1017/jfm.2016.447 Published online by Cambridge University Press

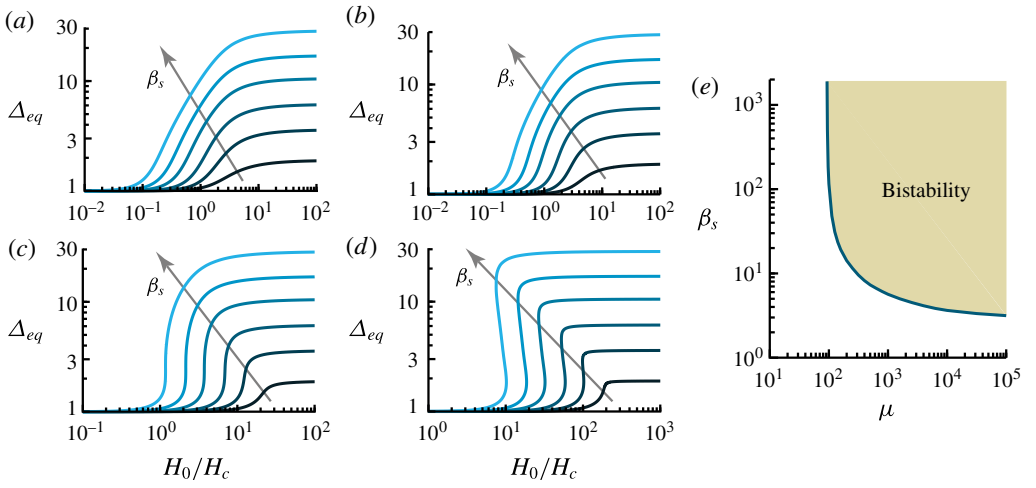


FIGURE 3. (Colour online) Equilibrium aspect ratio Δ_{eq} as a function of H_0/H_c for $\mu = 1, 10, 100, 1000$ (a, b, c, d, respectively), where $\mu = M_s/H_c$ is the ratio of saturation magnetization to saturation field. For each value of μ, solutions for values of $\beta_s = 3, 10, 30, 100, 300, 1000$ are shown, with the lower curves corresponding to smaller β_s. (e) Parameter space indicating the region of drop shape bistability.

In figure 3 we show the dependence of the equilibrium drop aspect ratio on the externally applied magnetic field H_0 for different values of μ and β_s. For small enough values of μ (figure 3*a*,*b*), the aspect ratio increases monotonically with the applied magnetic field H_0, and saturates for large values of H_0/H_c, as the magnetization saturates in this limit and so does the magnetic stress. As μ is increased above a critical value, there exist values of β_s for which there is a bistability of drop shapes within a range of values of the applied magnetic field H_0 (figure 3*c*,*d*). The range of the parameters μ and β_s for which drop shape bistability occurs is shown in figure 3(e). No shape bistability exists below a critical value of μ. While there are qualitative differences between the linear and nonlinear ferrofluid regimes (as also noted by Basaran & Wohlhuter (1992)), the bistability threshold of μ is analogous to the bistability threshold of permeability and permittivity for linear ferrofluid (Bacri & Salin 1982) and dielectric (Rosenkilde 1969; Miksis 1981; Wohlhuter & Basaran 1992) drops, respectively.

The shape bistability diagram in figure 3(e) can be explored experimentally using ferrofluids composed of monodisperse magnetic nanoparticles. Varying the size and volume fraction of the nanoparticles enables controlled changes of the parameter μ through its dependence on H_c and M_s, respectively (see Rosensweig (2013) for more details on the Langevin ferrofluid parameters). The parameter β_s can be varied independently of μ by changing the radius R of the drop, without changing the properties of the ferrofluid.

Regardless of the specific ferrofluid used, no instability due to sharp conical tips is observed in our solutions. This is because, in the limit of non-magnetic media considered here, the magnetic stress is independent of the large field outside the drop at the poles and remains finite (see (3.1)). However, dynamic Rayleigh-type instabilities may cause drop breakups when deformations are large (Sherwood 1988; Basaran *et al.* 1995; Potts *et al.* 2001; Lac & Homsy 2007; Afkhami *et al.* 2008;

https://doi.org/10.1017/jfm.2016.447 Published online by Cambridge University Press

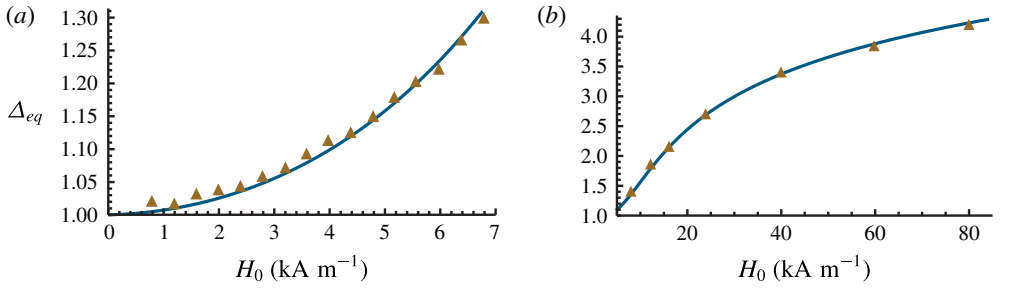


FIGURE 4. (Colour online) Dependence of the equilibrium drop aspect ratio on the externally applied field H_0 for low (a) and high (b) magnetic fields. Triangles show the measured values obtained by Afkhami *et al.* (2010) and solid curves show fits to these data obtained from our theoretical analysis (solutions of (3.1)), using the magnetization curves reported in Afkhami *et al.* (2010) ($M = 0.8903H + 0.1634$ for the linear magnetization regime (a) and $M = 4.8568\ \ln(H) - 3.956$ for the nonlinear magnetization regime (b), both in kA m^{-1}). Using the unperturbed drop radius $R = 1.291$ mm reported by Afkhami *et al.* (2010), the values of interfacial tension obtained from the fits are $\gamma = 18.2$ mN m^{-1} and $\gamma = 17.5$ mN m^{-1} for the low (a) and high (b) magnetic fields.

Paknemat *et al.* 2012). Also, the drop–medium interface may be destabilized for large enough magnetic fields (Boudouvis *et al.* 1987). We have not studied these instabilities in this work.

3.2. *Comparison of equilibrium deformations with previous experiments*

Various experimental works have studied the deformation of ferrofluid drops as a function of experimentally controlled parameters, such as the applied magnetic field. To explore the importance of considering the exact drop shapes and also to address discrepancies between previous theoretical and experimental results, we compare our numerical predictions to experimental observations of equilibrium drop deformation in both linear and nonlinear ferrofluid regimes by Afkhami *et al.* (2010). The theoretical description in Afkhami *et al.* (2010) was able to accurately reproduce the observed dependence of the drop aspect ratio with the applied magnetic field for small magnetic fields (small deformations) assuming ellipsoidal drop shapes. However, for large magnetic fields (large deformations), the measured dependence of the drop aspect ratio on the applied magnetic field could not be explained by the theoretical or numerical results of that work, even when *ad hoc* assumptions, such as a field-dependent interfacial tension γ, were considered. We re-evaluate this discrepancy in Afkhami *et al.* (2010) using our theoretical description, which does not assume ellipsoidal drop shapes and accounts for the exact drop shape.

Figures 4(a) and 4(b) show the dependence of the drop aspect ratio on the applied magnetic field measured by Afkhami *et al.* (2010), together with our numerical results, which were computed using the magnetization curves measured in Afkhami *et al.* (2010). Importantly, fitting the experimental data independently in the linear and nonlinear regimes of the ferrofluid (using the value of unperturbed drop radius reported in Afkhami *et al.* (2010)), we obtain the same value of the drop interfacial tension. Specifically, the values of the interfacial tension obtained from the fits are $\gamma = 18.2$ mN m^{-1} and $\gamma = 17.5$ mN m^{-1} for the low- and

https://doi.org/10.1017/jfm.2016.447 Published online by Cambridge University Press

high-magnetic-field regimes, respectively, which differ by roughly 3 % and are well within the experimental errors in Afkhami *et al.* (2010). Our theoretical description is thus able to reproduce the experimental data for both low and high magnetic fields (linear and nonlinear magnetization regimes) using a single value of the interfacial tension. Our analysis indicates that the discrepancy between theoretical predictions and observations at large values of the magnetic field in Afkhami *et al.* (2010) was due to the ellipsoidal shape approximation.

4. Dynamics of ferrofluid drop deformation

In contrast to the equilibrium drop shapes, the dynamics of ferrofluid drop deformations involves fluid flows inside and outside the drop and, therefore, it depends on both β and the viscosity ratio λ. The equations that govern the dynamics of drop shape deformation and fluid flows in the system were derived in § 2 ((2.1)–(2.5)). Analytical treatment of this free boundary problem is complex and only possible in some limiting regimes. Instead, we numerically integrate them using the Two Phase Fluid Moving Mesh module of COMSOL Multiphysics V5.0. We use a hybrid approach and solve numerically only for the hydrodynamic fields by including the analytical values of the magnetic stresses $\sigma_m \cos^2 \alpha$ and σ_i (see § 2) as normal stresses at the drop interface. We have checked that this hybrid method yields the same results as the full numerical solution including both magnetic and hydrodynamic fields, but it is considerably better in terms of computational efficiency. In addition to significantly reducing the simulation time, this approach also reduces numerical errors and instabilities by using a smooth analytical function for the magnetic stress at the drop interface.

4.1. *Dynamics of drop relaxation*

We consider first an initially deformed drop that relaxes towards its final equilibrium spherical shape. Such drop relaxation in the absence of any magnetic field corresponds to $\beta = 0$ and, therefore, relaxation dynamics depends solely on the viscosity ratio λ. To allow meaningful comparisons with previous theoretical works, which assumed ellipsoidal drop shapes (Rallison 1984), we consider, in this section, the drop relaxation from an ellipsoidal shape. We have checked that the results shown below do not change qualitatively if the initial drop shape is set to its exact equilibrium shape (under a magnetic field) instead of an ellipsoid. In particular, the changes are negligible for small and moderate values of β, as the equilibrium drop shapes are close to ellipsoids in this limit (figure 2).

Figure 5 shows the time evolution of the drop deformation, quantified by their deformation factor $D \equiv (b - a)/(b + a)$ (Rallison 1984), during relaxation towards the spherical equilibrium shape, for different values of initial deformation D_0 and λ. For small initial drop deformations (figure 5*a*), the deformation factor D decays exponentially with a λ-dependent relaxation time scale τ_R (figure 5*b*). Our numerical results agree perfectly with the analytical prediction $\tau_R(\lambda) = \tau_m(2\lambda + 3)(19\lambda + 16)/(40(\lambda + 1))$ for drop relaxation from small initial deformations (Rallison 1984, figure 5*b*). As the initial drop deformation becomes finite, the decay of deformation factor $D(t)$ deviates from the exponential decay as long as the drop shape deformations remain finite. Once drop deformation reaches small enough values, $D(t)$ decays exponentially with the same D_0-independent time scale τ_R (figure 5*c*,*d*, insets). While $D(t)$ deviates substantially from a single-exponential decay for even mild deformations ($D \gtrsim 0.1$ or $\Delta \gtrsim 1.2$), the quantity $\delta \equiv b/a - 1$ displays an

https://doi.org/10.1017/jfm.2016.447 Published online by Cambridge University Press

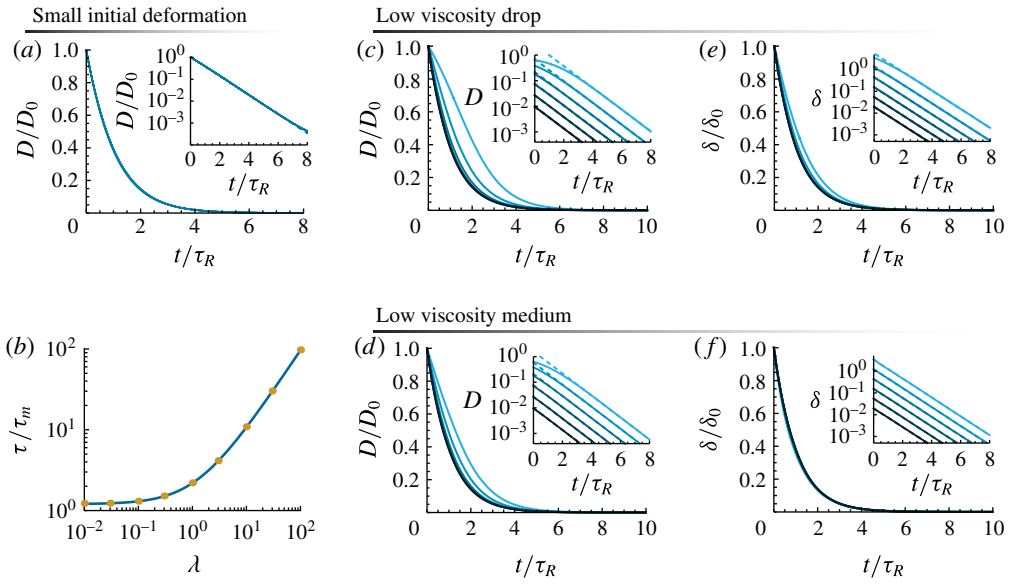


FIGURE 5. (Colour online) (*a*) Time evolution of the deformation factor $D(t)$ for a drop relaxing towards its final spherical state starting from a barely deformed initial ellipsoidal drop ($D_0 \approx 0.091$ or $\Delta_0 = 1.2$) for viscosity ratio $\lambda = 10^{-2}$–10^2, and (*b*) their decay time scales τ as a function of λ. Solid line and points in (*b*) correspond to the theoretical result ($\tau_R = \tau_m(2\lambda+3)(19\lambda+16)/(40(\lambda+1))$; Rallison (1984)), and our numerical value of τ, respectively. (*c*,*d*) Plots of $D(t)$ for finite initial deformations: $D_0 \approx 0.007$–0.47 for (*c*) $\lambda \ll 1$ and (*d*) $\lambda \gg 1$. (*e*,*f*) Plots of $\delta(t)$ of the same simulations as in (*c*) and (*d*) with initial values $\delta_0 \approx 0.014$–3.5 for (*e*) $\lambda \ll 1$ and (*f*) $\lambda \gg 1$.

exponential decay with the same characteristic time scale τ_R for significantly larger initial drop deformations (figure 5*e*,*f*), especially for relatively low-viscosity external media ($\lambda \gg 1$).

4.2. *Dynamics of drop deformation from an initially undeformed spherical shape*

We simulate an initially undeformed spherical ferrofluid drop actuated at time $t = 0$ with a spatially uniform magnetic field and analyse the dynamics of its deformation towards its equilibrium deformed shape (equilibrium deformation obtained in simulations shown as black dots in figure 2*c*). The actuation dynamics, which we analyse below using the quantity $\delta(t)$ (equivalent to the drop aspect ratio), depends on both β and λ.

For small values of β, corresponding to small final (equilibrium) drop deformations, the dynamics of drop deformation is exponential, namely $\delta(t) \simeq (\beta/4)(1 - \exp(t/\tau_R))$, where τ_R is the β-independent relaxation time scale obtained previously for drop relaxations (figure 5*b*), and $\beta/4$ is the equilibrium deformation for small values of β (from (3.2) or from Tsebers (1985)). This is due to a negligible change in the magnetic stress during deformation, time reversibility of Stokes flow and the nearly spherical final drop shape for small applied magnetic field (small β).

For larger values of β, the exponential relation above only holds for $t \ll \tau_R$ (while the drop deformations are still relatively small), leading to the linear relation $\delta(t) \simeq$

https://doi.org/10.1017/jfm.2016.447 Published online by Cambridge University Press

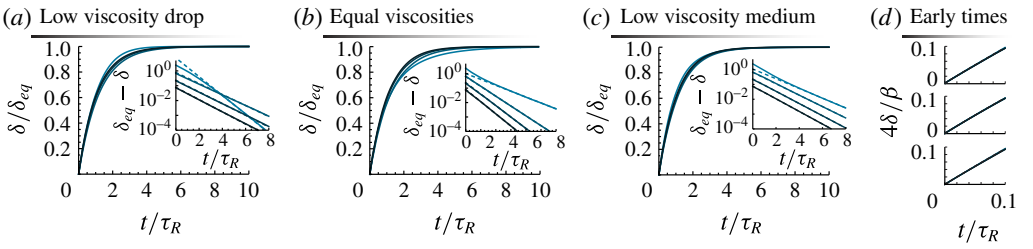


FIGURE 6. (Colour online) Time evolution of $\delta(t)$ in the saturation magnetization regime for various values of $\beta_s = 0.28,\ 0.80,\ 2.3,\ 9.1$ (darker colour corresponds to smaller β_s) and (*a*) $\lambda \ll 1$, (*b*) $\lambda = 1$ and (*c*) $\lambda \gg 1$. The insets show $\delta_{eq} - \delta(t)$ versus time in log scale with the fitted exponentials at long times (dashed lines). (*d*) Same $\delta(t)$ curves normalized with $\beta_s/4$ at early times $t \ll \tau_R$.

$(\beta/4)(t/\tau_R)$ at early times (figure 6*d*). Specifically,

$$\delta(t) \simeq \frac{10(\lambda+1)}{(2\lambda+3)(19\lambda+16)} \frac{t}{(\eta_m/\sigma_m)}, \tag{4.1}$$

which is independent of the capillary stresses because the drop deformation is much smaller than its equilibrium value δ_{eq} at these early times, and the restoring capillary stresses are small compared to the magnetic stresses. As time goes on, the droplet gets increasingly deformed and $\delta(t)$ crosses over to another exponential regime with a β- and λ-dependent time scale τ as it approaches its (final) equilibrium state (figure 6, insets). The time scale τ of this final exponential approach depends on both λ and β only for large β and, therefore, τ deviates from τ_R only when the final equilibrium drop shape deviates substantially from spherical. To analyse the changes of the time scale τ to reach the final equilibrium drop shape, we study the ratio τ/τ_R for distinct regimes of the ferrofluid and limiting viscosity ratios λ (figure 7).

As mentioned in § 3.1, the relation between the magnetization of a Langevin ferrofluid and the applied field H_0 involves two dimensionless parameters, namely, $\beta_s = \mu_0 M_s^2 R/2\gamma$ and $\mu = M_s/H_c$. Therefore, for an arbitrary field, which can span the full nonlinear regime of the magnetization curve of the ferrofluid, the dynamics of drop deformation is controlled by all the dimensionless parameters λ, β_s and μ, as well as by the value of the external magnetic field H_0. Figure 7(*a*) shows the dependence of the normalized time scale τ/τ_R on the applied magnetic field H_0, for different values of μ and β_s and limiting regimes of λ. We restrict our analysis to a fixed value $\mu \sim 1$ for simplicity and to avoid complications due to the bistability of equilibrium shapes (see § 3.1). We have checked that the results are qualitatively the same for other values of μ, as long as $\mu \sim 1$.

For small enough applied magnetic fields ($H_0 \ll H_c$), the drop magnetization $M = \chi H$ increases linearly with the magnetic field H in the drop (and consequently with the applied field H_0), where $\chi = \mu/3$ is the magnetic susceptibility. In this linear regime, the dynamics of drop deformation depends only on λ, $\mu = 3\chi$ and the 'Bond number' $\beta_0 \equiv \mu_0 H_0^2 R/2\gamma$ (Afkhami *et al.* 2010), which is equivalent to the applied field H_0. Figure 7(*b*) shows the dependence of τ/τ_R on β_0 for limiting cases of λ and fixed $\mu \sim 1$.

For large applied magnetic fields ($H_0 \gg H_c$), the drop magnetization saturates to the value M_s and remains constant during the drop deformation. In this saturation regime,

https://doi.org/10.1017/jfm.2016.447 Published online by Cambridge University Press

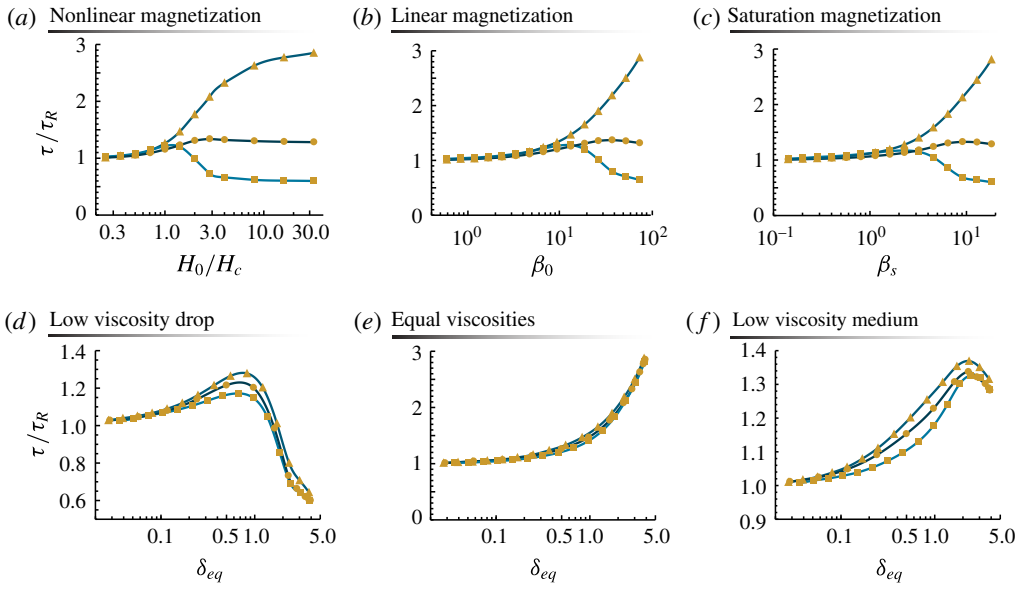


FIGURE 7. (Colour online) (*a–c*) Normalized time scale τ/τ_R of the final approach of the drops to their deformed equilibrium shapes as a function of H_0/H_c, β_0 and β_s for (*a*) nonlinear, (*b*) linear and (*c*) saturation ferrofluid regimes, and $\lambda \ll 1$ (squares), $\lambda = 1$ (triangles) and $\lambda \gg 1$ (circles). A smooth cubic spline curve passes through the points. (*d–f*) Normalized time scale τ/τ_R as a function of the final equilibrium drop deformation δ_{eq} for the limiting cases (*d*) $\lambda \ll 1$, (*e*) $\lambda = 1$ and (*f*) $\lambda \gg 1$. Saturation, linear and nonlinear ferrofluid regimes correspond to squares, triangles and circles, respectively.

the time scale τ is independent of H_0 and depends only on λ and β_s. Figure 7(*c*) shows the dependence of τ/τ_R on β_s for different limiting cases of the viscosity ratio λ.

In all ferrofluid regimes (saturation, linear and nonlinear), the deviation of τ from τ_R is of order one for a wide range of equilibrium drop deformations and viscosity ratios λ, indicating that the characteristic time scale of drop deformation towards the equilibrium shape is essentially determined by τ_R. In the cases where either the drop or the external medium have relatively low viscosity (figure 7*d*,*f*), the deviation of τ from τ_R is smallest, whereas in the intermediate regime (figure 7*e*), in which the two fluids have the same viscosity ($\lambda = 1$), the deviations are largest. The time scale τ depends only weakly on the specific ferrofluid regime and is essentially determined by the final deformation δ_{eq} of the drop, which is controlled by the ratio of magnetic to capillary stresses β_s and the value of the magnetic field, as described above (figure 7*d–f*).

5. Discussion

In this work, we provided a systematic analysis of the deformation dynamics of a Newtonian ferrofluid drop in a viscous fluid when actuated by spatially uniform magnetic fields. We solved for the exact equilibrium drop shapes as a function of the only relevant dimensionless parameter in the problem, namely the ratio β of magnetic to capillary stresses, for arbitrary physicochemical properties of the ferrofluids. We showed that drop shapes are nearly ellipsoidal for small to intermediate values of β,

https://doi.org/10.1017/jfm.2016.447 Published online by Cambridge University Press

but that these deviate significantly from ellipsoidal shapes as β is increased, specially at the drop tips. We also showed that the dependence of the equilibrium drop shape on the externally applied magnetic field shows a shape bistability, as previously reported, but only for highly susceptible ferrofluids that are rarely used in most practical applications. In addition, we solve the dynamics of ferrofluid drop deformations in viscous Newtonian fluids when actuated by uniform magnetic fields. The dynamics is obtained for arbitrary ferrofluids (nonlinear and linear magnetizations) as well as for finite drop deformations. We show that the dynamics of drop deformation by an applied uniform magnetic field is controlled by the same time scale as the drop relaxation in the absence of magnetic field, up to a numerical factor that essentially depends on the viscosity ratio and the ratio of magnetic stress to capillary stress. These results were obtained with a computational scheme that we developed using COMSOL Multiphysics V5.0 and allows computationally efficient simulations of the drop dynamics under various conditions. The versatility of this computational scheme will enable the study of ferrofluid drop actuation in a wide range of situations, from viscoelastic fluids to diverse temporal magnetic actuations of the drops.

Our results can be used for many practical applications requiring a detailed understanding of ferrofluid drop dynamics, including biomedical applications such as drug delivery (Gupta & Gupta 2005; Bychkova *et al.* 2012), where shape-dependent particle uptake has been observed (Champion & Mitragotri 2006). Also, precise measurements of the drop dynamics and equilibrium shapes would enable precise local measurements of both the viscosity of the external medium (or the drop) and the drop interfacial tension.

Acknowledgements

We thank G. Leal for fruitful discussions. P.R. thanks the Santa Barbara Foundation and the Errett Fisher Foundation for financial support.

REFERENCES

ABOU, B., WESFREID, J.-E. & ROUX, S. 2000 The normal field instability in ferrofluids: hexagon–square transition mechanism and wavenumber selection. *J. Fluid Mech.* **416**, 217–237.

ACERO, A. J., FERRERA, C., MONTANERO, J. M., HERRADA, M. A. & LÓPEZ-HERRERA, J. M. 2013 Experimental analysis of the evolution of an electrified drop following high voltage switching. *Eur. J. Mech.* (B/*Fluids)* **38**, 58–64.

AFKHAMI, S., RENARDY, Y., RENARDY, M., RIFFLE, J. S. & ST PIERRE, T. 2008 Field-induced motion of ferrofluid droplets through immiscible viscous media. *J. Fluid Mech.* **610**, 363–380.

AFKHAMI, S., TYLER, A. J., RENARDY, Y., RENARDY, M., ST PIERRE, T. G., WOODWARD, R. C. & RIFFLE, J. S. 2010 Deformation of a hydrophobic ferrofluid droplet suspended in a viscous medium under uniform magnetic fields. *J. Fluid Mech.* **663**, 358–384.

ALLAN, R. S. & MASON, S. G. 1962 Particle behaviour in shear and electric fields. I. Deformation and burst of fluid drops. *Proc. R. Soc. Lond.* A **267** (1328), 45–61.

ARKHIPENKO, V. I., BARKOV, Y. D. & BASHTOVOI, V. G. 1979 Shape of a drop of magnetized fluid in a homogeneous magnetic field. *Magn. Gidrodin.* **14**, 131–134.

BACRI, J.-C., CEBERS, A. O. & PERZYNSKI, R. 1994 Behavior of a magnetic fluid microdrop in a rotating magnetic field. *Phys. Rev. Lett.* **72** (17), 2705–2708.

BACRI, J. C. & SALIN, D. 1982 Instability of ferrofluid magnetic drops under magnetic field. *J. Phys. Lett.* **43** (17), 649–654.

BASARAN, O. A., PATZEK, T. W., BENNER, R. E. JR & SCRIVEN, L. E. 1995 Nonlinear oscillations and breakup of conducting, inviscid drops in an externally applied electric field. *Ind. Engng Chem. Res.* **34** (10), 3454–3465.

https://doi.org/10.1017/jfm.2016.447 Published online by Cambridge University Press

BASARAN, O. A. & WOHLHUTER, F. K. 1992 Effect of nonlinear polarization on shapes and stability of pendant and sessile drops in an electric (magnetic) field. *J. Fluid Mech.* **244**, 1–16.

BOUDOUVIS, A. G., PUCHALLA, J. L., SCRIVEN, L. E. & ROSENSWEIG, R. E. 1987 Normal field instability and patterns in pools of ferrofluid. *J. Magn. Magn. Mater.* **65** (2), 307–310.

BYCHKOVA, A. V., SOROKINA, O. N., ROSENFELD, M. A. & KOVARSKI, A. L. 2012 Multifunctional biocompatible coatings on magnetic nanoparticles. *Russ. Chem. Rev.* **81** (11), 1026–1050.

CAO, Y. & DING, Z. J. 2014 Formation of hexagonal pattern of ferrofluid in magnetic field. *J. Magn. Magn. Mater.* **355**, 93–99.

CEBERS, A. & KALIS, H. 2012 Mathematical modelling of an elongated magnetic droplet in a rotating magnetic field. *Math. Modelling Numer. Anal.* **17** (1), 47–57.

CHAMPION, J. A. & MITRAGOTRI, S. 2006 Role of target geometry in phagocytosis. *Proc. Natl Acad. Sci. USA* **103** (13), 4930–4934.

CHEN, C.-Y., CHEN, C.-H. & LEE, W.-F. 2009 Experiments on breakups of a magnetic fluid drop through a micro-orifice. *J. Magn. Magn. Mater.* **321** (20), 3520–3525.

CHEN, C.-Y. & CHENG, Z.-Y. 2008 An experimental study on Rosensweig instability of a ferrofluid droplet. *Phys. Fluids* **20** (5), 054105.

CHILCOTT, M. D. & RALLISON, J. M. 1988 Creeping flow of dilute polymer solutions past cylinders and spheres. *J. Non-Newtonian Fluid Mech.* **29**, 381–432.

COLLINS, R. T., HARRIS, M. T. & BASARAN, O. A. 2007 Breakup of electrified jets. *J. Fluid Mech.* **588**, 75.

CORSON, L. T., TSAKONAS, C., DUFFY, B. R., MOTTRAM, N. J., SAGE, I. C., BROWN, C. V. & WILSON, S. K. 2014 Deformation of a nearly hemispherical conducting drop due to an electric field: theory and experiment. *Phys. Fluids* **26** (12), 122106.

COX, R. G. 1969 The deformation of a drop in a general time-dependent fluid flow. *J. Fluid Mech.* **37** (03), 601–623.

DATTA, S., DAS, A. K. & DAS, P. K. 2015 Uphill movement of sessile droplets by electrostatic actuation. *Langmuir* **31** (37), 10190–10197.

DESHMUKH, S. D. & THAOKAR, R. M. 2012 Deformation, breakup and motion of a perfect dielectric drop in a quadrupole electric field. *Phys. Fluids* **24** (3), 032105.

ENGEL, A., LANGER, H. & CHETVERIKOV, V. 1999 Non-linear analysis of the surface profile resulting from the one-dimensional Rosensweig instability. *J. Magn. Magn. Mater.* **195** (1), 212–219.

ESMAEELI, A. & SHARIFI, P. 2011*a* The transient dynamics of a liquid column in a uniform transverse electric field of small strength. *J. Electrostat.* **69** (6), 504–511.

ESMAEELI, A. & SHARIFI, P. 2011*b* Transient electrohydrodynamics of a liquid drop. *Phys. Rev.* E **84** (3), 036308.

FENG, J. Q. & SCOTT, T. C. 1996 A computational analysis of electrohydrodynamics of a leaky dielectric drop in an electric field. *J. Fluid Mech.* **311**, 289–326.

FERRERA, C., LÓPEZ-HERRERA, J. M., HERRADA, M. A., MONTANERO, J. M. & ACERO, A. J. 2013 Dynamical behavior of electrified pendant drops. *Phys. Fluids* **25** (1), 012104.

FRIBERG, S., LARSSON, K. & SJOBLOM, J. 2003 *Food Emulsions*. CRC Press.

GOLLWITZER, C., MATTHIES, G., RICHTER, R., REHBERG, I. & TOBISKA, L. 2007 The surface topography of a magnetic fluid: a quantitative comparison between experiment and numerical simulation. *J. Fluid Mech.* **571**, 455–474.

GUPTA, A. K. & GUPTA, M. 2005 Synthesis and surface engineering of iron oxide nanoparticles for biomedical applications. *Biomaterials* **26** (18), 3995–4021.

KARYAPPA, R. B., NAIK, A. V. & THAOKAR, R. M. 2015 Electroemulsification in a uniform electric field. *Langmuir* **32** (1), 46–54.

KUMAR, C. S. S. R. & MOHAMMAD, F. 2011 Magnetic nanomaterials for hyperthermia-based therapy and controlled drug delivery. *Adv. Drug Deliv. Rev.* **63** (9), 789–808.

KUSHCH, V. I., SANGANI, A. S., SPELT, P. D. M. & KOCH, D. L. 2002 Finite-Weber-number motion of bubbles through a nearly inviscid liquid. *J. Fluid Mech.* **460**, 241–280.

LAC, E. & HOMSY, G. M. 2007 Axisymmetric deformation and stability of a viscous drop in a steady electric field. *J. Fluid Mech.* **590**, 239–264.

https://doi.org/10.1017/jfm.2016.447 Published online by Cambridge University Press

LANAUZE, J. A., WALKER, L. M. & KHAIR, A. S. 2015 Nonlinear electrohydrodynamics of slightly deformed oblate drops. *J. Fluid Mech.* **774**, 245–266.

LANDAU, L. D., PITAEVSKII, L. P. & LIFSHITZ, E. M. 1984 *Electrodynamics of Continuous Media*. Elsevier.

LAURENT, S., DUTZ, S., HÄFELI, U. O. & MAHMOUDI, M. 2011 Magnetic fluid hyperthermia: focus on superparamagnetic iron oxide nanoparticles. *Adv. Colloid Interface Sci.* **166** (1), 8–23.

LAVROVA, O., MATTHIES, G., MITKOVA, T., POLEVIKOV, V. & TOBISKA, L. 2006 Numerical treatment of free surface problems in ferrohydrodynamics. *J. Phys.: Condens. Matter* **18** (38), S2657–S2669.

LAVROVA, O., MATTHIES, G., POLEVIKOV, V. & TOBISKA, L. 2004 Numerical modeling of the equilibrium shapes of a ferrofluid drop in an external magnetic field. *Proc. Appl. Maths Mech.* **4** (1), 704–705.

LI, H., HALSEY, T. C. & LOBKOVSKY, A. 1994 Singular shape of a fluid drop in an electric or magnetic field. *Europhys. Lett.* **27** (8), 575.

MANDAL, S., CHAUDHURY, K. & CHAKRABORTY, S. 2014 Transient dynamics of confined liquid drops in a uniform electric field. *Phys. Rev.* E **89** (5), 053020.

MEIRON, D. I. 1989 On the stability of gas bubbles rising in an inviscid fluid. *J. Fluid Mech.* **198**, 101–114.

MELCHER, J. R. & TAYLOR, G. I. 1969 Electrohydrodynamics: a review of the role of interfacial shear stresses. *Annu. Rev. Fluid Mech.* **1**, 111–146.

MIKSIS, M. J. 1981 Shape of a drop in an electric field. *Phys. Fluids* **24** (11), 1967–1972.

MIZUTA, Y. 2011 Stability analysis on the free surface phenomena of a magnetic fluid for general use. *J. Magn. Magn. Mater.* **323** (10), 1354–1359.

NGUYEN, N.-T., NG, K. M. & HUANG, X. 2006 Manipulation of ferrofluid droplets using planar coils. *Appl. Phys. Lett.* **89** (5), 052509.

NIELLOUD, F. & MARTI-MESTRES, G. 2000 *Pharmaceutical Emulsions and Suspensions: Revised and Expanded*. CRC Press.

NOTZ, P. K. & BASARAN, O. A. 1999 Dynamics of drop formation in an electric field. *J. Colloid Interface Sci.* **213** (1), 218–237.

PAKNEMAT, H., PISHEVAR, A. R. & POURNADERI, P. 2012 Numerical simulation of drop deformations and breakup modes caused by direct current electric fields. *Phys. Fluids* **24** (10), 102101.

PILLAI, R., BERRY, J. D., HARVIE, D. J. E. & DAVIDSON, M. R. 2015 Electrolytic drops in an electric field: a numerical study of drop deformation and breakup. *Phy. Rev.* E **92** (1), 013007.

POTTS, H. E., BARRETT, R. K. & DIVER, D. A. 2001 Dynamics of freely-suspended drops. *J. Phys.* D: *Appl. Phys.* **34** (17), 2529.

RALLISON, J. M. 1984 The deformation of small viscous drops and bubbles in shear flows. *Annu. Rev. Fluid Mech.* **16** (1), 45–66.

RAMASWAMY, S. & LEAL, L. G. 1999 The deformation of a newtonian drop in the uniaxial extensional flow of a viscoelastic liquid. *J. Non-Newtonian Fluid Mech.* **88** (1), 149–172.

RHODES, S., HE, X., ELBORAI, S., LEE, S.-H. & ZAHN, M. 2006 Magnetic fluid behavior in uniform dc, ac, and rotating magnetic fields. *J. Electrostat.* **64** (7), 513–519.

ROSENKILDE, C. E. 1969 A dielectric fluid drop in an electric field. *Proc. R. Soc. Lond.* A **312** (1511), 473–494.

ROSENSWEIG, R. E. 2013 *Ferrohydrodynamics*. Courier Corporation.

SALIPANTE, P. F. & VLAHOVSKA, P. M. 2010 Electrohydrodynamics of drops in strong uniform dc electric fields. *Phys. Fluids* **22** (11), 112110.

SAVILLE, D. A. 1997 Electrohydrodynamics: the Taylor–Melcher leaky dielectric model. *Annu. Rev. Fluid Mech.* **29**, 27–64.

SCHMITZ, R. & FELDERHOF, B. U. 1982 Creeping flow about a spherical particle. *Physica* A **113** (1), 90–102.

SERO-GUILLAUME, O. E., ZOUAOUI, D., BERNARDIN, D. & BRANCHER, J. P. 1992 The shape of a magnetic liquid drop. *J. Fluid Mech.* **241**, 215–232.

https://doi.org/10.1017/jfm.2016.447 Published online by Cambridge University Press

SHAPIRO, B., KULKARNI, S., NACEV, A., MURO, S., STEPANOV, P. Y. & WEINBERG, I. N. 2015 Open challenges in magnetic drug targeting. *WIREs Nanomed. Nanobiotechnol.* **7** (3), 446–457.

SHAW, S. J. & SPELT, P. D. M. 2009 Critical strength of an electric field whereby a bubble can adopt a steady shape. *Proc. R. Soc. Lond.* A **465**, 3127–3143.

SHERWOOD, J. D. 1988 Breakup of fluid droplets in electric and magnetic fields. *J. Fluid Mech.* **188**, 133–146.

SHERWOOD, J. D. 1991 The deformation of a fluid drop in an electric field: a slender-body analysis. *J. Phys.* A*: Math. Gen.* **24** (17), 4047.

SHI, D., BI, Q. & ZHOU, R. 2014 Numerical simulation of a falling ferrofluid droplet in a uniform magnetic field by the VOSET method. *Numer. Heat Transfer* **66** (2), 144–164.

SHLIOMIS, M. I. 1972 Effective viscosity of magnetic suspensions. *Zh. Eksp. Teor. Fiz.* **61**, 2411–2418.

SJOBLOM, J. 2005 *Emulsions and Emulsion Stability. (Surfactant Science Series)*, vol. 132. CRC Press.

STIERSTADT, K. & LIU, M. 2015 Maxwell's stress tensor and the forces in magnetic liquids. *Z. Angew. Math. Mech.* **95** (1), 4–37.

STONE, H. A., LISTER, J. R. & BRENNER, M. P. 1999 Drops with conical ends in electric and magnetic fields. *Proc. R. Soc. Lond.* A **455** (1981), 329–347.

TAYLOR, G. I. 1934 The formation of emulsions in definable fields of flow. *Proc. R. Soc. Lond.* A **146**, 501–523.

TAYLOR, G. I. 1964 Disintegration of water drops in an electric field. *Proc. R. Soc. Lond.* A **280** (1382), 383–397.

TRETHEWAY, D. C. & LEAL, L. G. 2001 Deformation and relaxation of Newtonian drops in planar extensional flows of a Boger fluid. *J. Non-Newtonian Fluid Mech.* **99** (2), 81–108.

TSEBERS, A. 1985 Virial method of investigation of statics and dynamics of drops of magnetizable liquids. *Magnetohydrodynamics (United States)* **21** (1), 19–26 (Engl. Transl.).

WEHKING, J. D. & KUMAR, R. 2015 Droplet actuation in an electrified microfluidic network. *Lab on a Chip* **15** (3), 793–801.

WOHLHUTER, F. K. & BASARAN, O. A. 1992 Shapes and stability of pendant and sessile dielectric drops in an electric field. *J. Fluid Mech.* **235**, 481–510.

WOHLHUTER, F. K. & BASARAN, O. A. 1993 Effects of physical properties and geometry on shapes and stability of polarizable drops in external fields. *J. Magn. Magn. Mater.* **122** (1), 259–263.

ZAKINYAN, A., NECHAEVA, O. & DIKANSKY, Y. 2012 Motion of a deformable drop of magnetic fluid on a solid surface in a rotating magnetic field. *Exp. Therm. Fluid Sci.* **39**, 265–268.

ZHOU, C., YUE, P., FENG, J. J., OLLIVIER-GOOCH, C. F. & HU, H. H. 2010 3D phase-field simulations of interfacial dynamics in Newtonian and viscoelastic fluids. *J. Comput. Phys.* **229** (2), 498–511.

ZHU, G.-P., NGUYEN, N.-T., RAMANUJAN, R. V. & HUANG, X.-Y. 2011 Nonlinear deformation of a ferrofluid droplet in a uniform magnetic field. *Langmuir* **27** (24), 14834–14841.

ZIMNY, K., MASCARO, B., BRUNET, T., PONCELET, O., ARISTÉGUI, C., LENG, J., SANDRE, O. & MONDAIN-MONVAL, O. 2014 Design of a fluorinated magneto-responsive material with tuneable ultrasound scattering properties. *J. Mater. Chem.* B **2** (10), 1285–1297.

https://doi.org/10.1017/jfm.2016.447 Published online by Cambridge University Press